

Nonsequential double ionization of Ne with elliptically polarized laser pulsesFang Liu ^{1,2,3,*}, Shuqi Li,⁴ Zhangjin Chen ⁴, Birger Böning,^{1,3} and Stephan Fritzsche ^{1,2,3}¹*Helmholtz-Institut Jena, 07743 Jena, Germany*²*Theoretisch-Physikalisches Institut, Friedrich-Schiller-Universität Jena, 07743 Jena, Germany*³*GSI Helmholtzzentrum für Schwerionenforschung GmbH, 64291 Darmstadt, Germany*⁴*Department of Physics, College of Science, Shantou University, 515063 Shantou, Guangdong, China*

(Received 13 July 2022; accepted 17 October 2022; published 31 October 2022)

We show through simulation that the improved quantitative rescattering model (QRS) can successfully predict the nonsequential double ionization (NSDI) process by intense elliptically polarized laser pulses. Using the QRS model, we calculate the correlated two-electron and ion momentum distributions of NSDI in Ne exposed to intense elliptically polarized laser pulses with a wavelength of 788 nm at a peak intensity of 5.0×10^{14} W/cm². We analyze the asymmetry in the doubly charged ion momentum spectra observed by Kang *et al.* [*Phys. Rev. Lett.* **120**, 223204 (2018)] in going from linearly to elliptically polarized laser pulses. Our model reproduces the experimental data well. Furthermore, we find that the ellipticity-dependent asymmetry arises from the drift velocity along the minor axis of the elliptic polarization. We explain how the correlated electron momentum distributions along the minor axis provide access to the subcycle dynamics of recollision. From these findings, we expect that we can extend the QRS model for NSDI toward more complicated laser fields in the future.

DOI: [10.1103/PhysRevA.106.043120](https://doi.org/10.1103/PhysRevA.106.043120)**I. INTRODUCTION**

As one of several important processes in strong-field physics, nonsequential double ionization (NSDI) of atoms has been studied both theoretically and experimentally for more than three decades. Experimentally, the major interest in NSDI stems from the first measurements of the total yield of doubly charged ions as a function of laser intensity if exposed to intense laser pulses [1–4]. The characteristic knee structure observed with increasing intensity provided distinct evidence for NSDI, since theoretical models based on the *sequential* emission of independent electrons predicted ion yields which are too small by several orders of magnitude. It was therefore concluded that a mechanism of nonsequential double ionization must be incorporated to describe the correlated dynamics of two electrons in a strong laser field.

However, in contrast to linearly polarized laser fields, the probability for NSDI will be strongly suppressed for elliptical polarization [5–9], since the transverse electric field component steers the initially emitted electron away from its parent ion. This expectation was supported also by earlier experimental studies [5], which measured the yield of doubly charged ions of Ne as a function of beam ellipticity. On the theoretical side, most previous attempts to describe the recollision mechanism in the NSDI with elliptically polarized beams have employed semiclassical or even fully classical ensemble methods [6,7]. In particular, Wang and Eberly applied the classical ensemble method to show that the so-called elliptical electron trajectories may lead to recollision in elliptically polarized beams [8].

Indeed, these earlier works have shown that an elliptical polarization may help control the recollision physics in strong-field ionization. Therefore, the NSDI process in elliptically polarized laser fields has been extensively investigated in experiments and it was found that not only does the total NSDI yield decrease significantly with increasing ellipticity but that the ion momentum distributions also change significantly. For example, Kang *et al.* [10] experimentally studied the correlated electron and doubly charged ion momenta for double ionization of Ne driven by elliptically polarized light and observed an ellipticity-dependent asymmetry of these distributions. Using a three-dimensional semiclassical model, they were able to simulate the correlated electron momentum distributions (CMDs) along the minor axis of elliptical polarization, and found that these CMDs provide access to distinguish recollisions before and after a zero-crossing of the laser electric field. Furthermore, it was argued that this may provide a means to obtain information about the recollision time [10].

Until now, the so-called quantitative rescattering (QRS) model [11,12] has exclusively been applied to treat NSDI in linearly polarized laser fields [13–16]. In recent years, however, many experimental and theoretical efforts have shifted to NSDI in elliptically polarized laser fields for which the semiclassical model has been widely employed. However, the QRS model, as a full quantum theory, is more accurate and more powerful in identifying the specific mechanisms of the NSDI process. Therefore, the QRS model may promise both an improved understanding of NSDI in elliptically polarized beams as well as more precise theoretical results.

In this paper, we extend the QRS model for NSDI towards elliptically polarized driving beams. With this extension, we compute the CMDs and ion momentum distributions and

*fang.liu@uni-jena.de

compare them to the experiment by Kang *et al.* [10]. In particular, we provide an explanation for the asymmetry in ion momentum distributions for large ellipticities. We show that the CMDs along the minor axis of polarization are a key to understanding this asymmetry. Essential to the rescattering picture is that there exists a laser-induced recolliding wave packet (RWP) which can initiate collisions with the ion core [17]. While the momentum distribution of the RWP cannot be directly measured, it can be theoretically deduced by the QRS model. Within the QRS model, the momentum distribution of RWP in elliptically polarized beams confirms that the initially emitted electrons propagate away from the parent ion. Based on this insight, we show that the QRS model reproduces the experimental values well, which confirms the relation between recollision time and ion momentum distributions clarified in Ref. [10]. These theoretical insights not only lead to quantitative explanations of previous and current experiments but also enhance the understanding of the underlying NSDI dynamics.

The paper is structured as follows. In Sec. II, we introduce the QRS model used to calculate the CMDs for NSDI with linearly polarized pulses and its extension towards elliptical polarization. Based on this model, the simulated results are shown and discussed in Sec. III. Finally, we present our conclusions and give an outlook for future work in Sec. IV.

Unless indicated otherwise, atomic units ($m_e = e = \hbar = 4\pi\epsilon_0 = 1$) are used throughout the paper.

II. THEORETICAL MODEL

We aim to calculate the CMDs and the ion momentum distributions for NSDI of Ne illuminated by intense linearly and elliptically polarized laser beams. After interaction with the beam, the atom is doubly ionized and two electrons are emitted with momenta \mathbf{p}_1 and \mathbf{p}_2 and are simultaneously measured at two detectors. The CMDs then refer to the momentum distributions of the two outgoing electrons along the major and minor polarization directions of the laser field.

The generally accepted mechanisms for NSDI are the laser-induced recollisional direct ionization (RDI) and the laser-induced recollisional excitation with subsequent ionization of the second electron from the excited state of the parent ion (RESI) [18]. According to the classical rescattering model, the maximum energy of the laser-induced returning electron in the experiments by Kang *et al.* [10] is about 95 eV, which is considerably larger than the ionization potential of Ne^+ (41 eV). Since the total cross sections for electron impact ionization of Ne^+ are much larger than those for electron impact excitation of Ne^+ (see Fig. 9 in Ref. [19]), the RDI dominates in NSDI of Ne and the contributions of RESI are negligible. For these reasons, we only consider RDI in the present work. Since the details of the improved QRS model for RDI have been presented in Refs. [16,20], only a brief summary of the methods used to simulate the CMD with a description of how to obtain the ion momentum distribution is given here.

The basic idea of the QRS model for RDI is that the CMD for the laser-induced RDI process in NSDI can be factorized into two parts, the RWP and the laser-free triple differential cross section (TDCS) for ionization of the parent ion by the impact of the laser-induced returning electron. Hereby, the

RWP is extracted from the two-dimensional (2D) momentum distributions for high-order above threshold ionization (HATI) photoelectrons calculated using the strong field approximation (SFA) theory [21]. For this purpose, we first briefly review the SFA theory for single ionization.

A. The strong-field approximation

Here we briefly review the SFA in the length gauge for single ionization in a strong laser field. The momentum-dependent transition amplitude can be written as a perturbation series in the atomic potential. The first two terms of this series are the so-called direct and rescattering amplitudes,

$$f_{\text{SFA}}(\mathbf{p}) = f_{\text{SFA1}}(\mathbf{p}) + f_{\text{SFA2}}(\mathbf{p}), \quad (1)$$

where \mathbf{p} is the momentum of the detected photoelectron. The direct ionization amplitude in Eq. (1) is given by [21,22]

$$f_{\text{SFA1}}(\mathbf{p}) = -i \int_{-\infty}^{\infty} dt \langle \chi_{\mathbf{p}}(t) | \mathbf{r} \cdot \mathbf{F}(t) | \Psi_i(t) \rangle, \quad (2)$$

where $\mathbf{F}(t)$ is the laser electric field that is elliptically polarized within the y - z plane,

$$\mathbf{F}(t) = F_0 \cos^2\left(\frac{\pi t}{\tau}\right) [\varepsilon_1 \cos(\omega t + \phi) \hat{\mathbf{z}} - \varepsilon_2 \sin(\omega t + \phi) \hat{\mathbf{y}}], \quad (3)$$

with the carrier frequency ω and the carrier-envelope phase ϕ for $-\tau/2 < t < \tau/2$, and is zero otherwise. The pulse duration, defined as the full width at half maximum (FWHM), is given by $\Gamma = \tau/2.75$. Furthermore, we defined $\varepsilon_1 = 1/(1 + \varepsilon^2)^{1/2}$ and $\varepsilon_2 = \varepsilon/(1 + \varepsilon^2)^{1/2}$, where $0 \leq \varepsilon \leq 1$ denotes the ellipticity. With this definition of the laser field, the y and z axes are the beam's minor and major axes, respectively.

In the direct transition amplitude [Eq. (2)], $\Psi_i(t)$ is the initial ground-state wave function, and $\chi_{\mathbf{p}}$ is a so-called Volkov state given by

$$\langle \mathbf{r} | \chi_{\mathbf{p}}(t) \rangle = \frac{1}{(2\pi)^{3/2}} e^{i[\mathbf{p} + \mathbf{A}(t)] \cdot \mathbf{r}} e^{-iS(\mathbf{p}, t)}, \quad (4)$$

where $\mathbf{A}(t)$ is the vector potential corresponding to the electric field [Eq. (3)], and the action S is given by

$$S(\mathbf{p}, t) = \frac{1}{2} \int_{-\infty}^t dt' [\mathbf{p} + \mathbf{A}(t')]^2. \quad (5)$$

The second term in the SFA transition amplitude [Eq. (1)], the so-called rescattering amplitude, accounts for laser-induced elastic scattering of the returning electron from the parent ion. This rescattering amplitude can be expressed as

$$f_{\text{SFA2}}(\mathbf{p}) = - \int_{-\infty}^{\infty} dt \int_t^{\infty} dt' \int d\mathbf{k} \langle \chi_{\mathbf{p}}(t') | V | \chi_{\mathbf{k}}(t') \rangle \times \langle \chi_{\mathbf{k}}(t) | \mathbf{r} \cdot \mathbf{F}(t) | \Psi_i(t) \rangle, \quad (6)$$

where V is the scattering potential. It takes the form

$$V(r) = \tilde{V}(r) e^{-\alpha r}, \quad (7)$$

where α is a screening factor introduced to avoid the singularity integrand in Eq. (6) and $\tilde{V}(r)$ is the atomic model potential that can be written in the form

$$\tilde{V}(r) = - \frac{1 + a_1 e^{-a_2 r} + a_3 r e^{-a_4 r} + a_5 e^{-a_6 r}}{r}. \quad (8)$$

The parameters a_i can be found in Ref. [23]. As can be seen from Eq. (6), the rescattering amplitude consists of three time-ordered steps by the electron: the initial tunnel ionization, propagation in the laser field, as well elastic scattering with the parent ion.

B. The recolliding wave packet

According to the QRS model, the momentum distribution of the HATI photoelectron with momentum \mathbf{p} can be factorized as a product of the RWP and the differential cross section (DCS) for elastic scattering of the returning electron from the parent ion [11]. This means the momentum distribution of the HATI photoelectron,

$$D_{\text{SFA2}}^{\text{HATI}}(\mathbf{p}) = |f_{\text{SFA2}}(\mathbf{p})|^2, \quad (9)$$

can be expressed as [21]

$$D_{\text{SFA2}}^{\text{HATI}}(\mathbf{p}) = W(k_r) \frac{d\sigma_{\text{PWBA}}^{\text{el}}(k_r, \theta_r)}{d\Omega_r}, \quad (10)$$

where $W(k_r)$ is the RWP that describes the momentum distribution of the returning electron with kinetic energy $E_r = k_r^2/2$, and $d\sigma_{\text{PWBA}}^{\text{el}}(k_r, \theta_r)/d\Omega_r$ is the DCS, which is calculated within the plane-wave first-order Born approximation (PWBA). For an electron with a momentum of magnitude k_r scattered at an angle θ_r with respect to the direction of momentum of the returning electron, it should be noted that the RWP is independent of the rescattering angle θ_r [11]. Within the classical rescattering model, we assumed that the electron returns along the major axis. The detected photoelectron momentum \mathbf{p} and the momentum \mathbf{k}_r of the scattered electron are related via [11]

$$\mathbf{p} = \mathbf{k}_r - \mathbf{A}_z(t_r), \quad (11)$$

with

$$k_r = 1.26|A_z(t_r)|, \quad (12)$$

where $\mathbf{A}_z(t_r)$ is the vector potential along the major axis at the recollision time t_r . The relation between k_r and $|A_z(t_r)|$ is determined approximately by solving Newton's equation of motion for an electron in a monochromatic laser field, and yields the factor 1.26 [11].

With the calculated HATI photoelectron momentum distribution and the DCS for elastic scattering of the returning electron with the parent ion, the momentum distribution of the RWP can be obtained by Eq. (10).

C. Recollision direct ionization

By applying the philosophy of the QRS model for the HATI process to the NSDI process, the correlated electron momentum distribution for RDI can be factorized as a product of the RWP and the parallel momentum distributions of the two outgoing electrons [13,14]. To simulate the CMDs for the laser-induced recollision ionization, one needs to have the TDCS corresponding to the laser-free ($e, 2e$) impact ionization on Ne^+ at all incident energies below the maximum returning electron energy with all possible outgoing angles. We apply the distorted-wave Born approximation (DWBA) [24] to calculate the required TDCS, which is less elaborate

when compared with other theoretical methods, such as the R-matrix method [25] and the convergent close-coupling (CCC) calculations [26]. This rather simple approach captures the main important features of the ($e, 2e$) impact ionization and typically gives rise to TDCS in fairly good agreement with measured data. However, the total cross sections (TCS) for low impact energies are often overestimated in the DWBA. Therefore, in this work, we also considered a special treatment by introducing a calibration procedure for DWBA [27].

The TDCS for the process of electron impact ionization at incident energy $E_i = k_i^2/2$ is given by

$$\frac{d^3\sigma}{d\Omega_1 d\Omega_2 dE_2} = (2\pi)^4 \frac{k_1 k_2}{k_i} \left[\frac{3}{4} |f(\mathbf{k}_1, \mathbf{k}_2) - g(\mathbf{k}_1, \mathbf{k}_2)|^2 + \frac{1}{4} |f(\mathbf{k}_1, \mathbf{k}_2) + g(\mathbf{k}_1, \mathbf{k}_2)|^2 \right], \quad (13)$$

where $\Omega_1(\theta_1, \phi_1)$ and $\Omega_2(\theta_2, \phi_2)$ refer to the solid angles of the two electrons with momenta \mathbf{k}_1 and \mathbf{k}_2 , and $g(\mathbf{k}_1, \mathbf{k}_2)$ is the exchange amplitude with $g(\mathbf{k}_1, \mathbf{k}_2) = f(\mathbf{k}_2, \mathbf{k}_1)$. In NSDI, the CMDs are typically only measured for the momentum components along the laser polarization axis for the two outgoing electrons. Thus, to compare with experiments, the calculated TDCS for the laser-free ($e, 2e$) process needs to be projected onto the polarization axis.

For a given incident energy, the calculated TDCS, in which the integrals over ϕ_1 and ϕ_2 have been performed, is originally a function of the energy $E_2 = k_2^2/2$ of the ejected electron and the scattering angles θ_1 and θ_2 of the two outgoing electrons. Due to the conservation of momentum, the TDCS can be converted to a function of k_{1z} , k_{2z} , and k_{1y} . Then the two-electron momentum spectra along the major polarization direction for the laser-free ($e, 2e$) process can be obtained by integrating the TDCS over k_{1y} ,

$$Y_{E_i}^{(e,2e)}(k_{1z}, k_{2z}) = \int_0^{k^{\max}} dk_{1y} \frac{d\sigma^3}{d\Omega_1 d\Omega_2 dE_2}(k_{1z}, k_{2z}, k_{1y}), \quad (14)$$

where $k^{\max} = \sqrt{2(E_i - I_p)}$, and I_p is the ionization potential of the parent ion Ne^+ .

For the laser-induced RDI process, the two electrons still feel the laser field after the collision and, hence, each electron will gain a drift momentum, which is determined mostly by the vector potential $A_j(t_r)$ ($j = \hat{x}, \hat{y}, \hat{z}$) at the time when the recollision takes place. Using the relation in Eq. (11) for each of the two outgoing electrons, the correlated two-electron momentum distributions parallel to the z axis for the RDI process in a strong field at an intensity I can be expressed as

$$D_{E_i, I}^{(\text{RDI})}(p_{1z}, p_{2z}) = Y_{E_i}^{(e,2e)}[k_{1z} - A_z(t_r), k_{2z} - A_z(t_r)], \quad (15)$$

where p_{1z} and p_{2z} are the parallel momenta of the two correlated electrons along the major laser polarization, respectively.

To obtain the CMD for a given intensity, one has to consider the contributions from all collisions at different incident energies weighted by the RWP. This gives

$$D_I^{(\text{RDI})}(p_{1z}, p_{2z}) = \int_{I_p}^{\infty} dE_i D_{E_i, I}^{(\text{RDI})}(p_{1z}, p_{2z}) W_I(E_i - \Delta E), \quad (16)$$

where $W_r(E_i - \Delta E)$ is the RWP that describes the energy distribution of the returning electron in the laser field at a single intensity I . Furthermore, ΔE is the lowering of threshold due to the presence of the electric field at the instant of recollision. It was argued by van der Hart and Burnett [28] that, in contrast to a field-free environment, the threshold energy for the laser-induced inelastic collision of the returning electron with the parent ion can be reduced by

$$\Delta E = 2\sqrt{Z_{\text{eff}}|F_r|}, \quad (17)$$

where F_r is the electric field at the time of collision. For the electron impact excitation and ionization of a singly charged ion, $Z_{\text{eff}} = 1$ and 2, respectively. With these empirical modifications in mind, Eq. (12) can be rewritten as

$$|A_z(t_r)| = \sqrt{2(E_i - \Delta E)}/1.26. \quad (18)$$

Finally, to compare directly with the experimental measurements, the focal-volume effect has to be considered. In the present simulations, therefore, the integral over the focal volume has been performed:

$$D_{I_0}^{(\text{RDI})}(p_{1z}, p_{2z}) = \int_0^{I_0} D_I^{(\text{RDI})}(p_{1z}, p_{2z}) \left(\frac{\partial V}{\partial I} \right) dI, \quad (19)$$

where I_0 is the peak intensity of the laser field, and $\frac{\partial V}{\partial I}$ is the volume of an iso-intensity shell. For a laser beam with a Lorentzian distribution in the propagation direction and a Gaussian distribution in the transverse direction, the volume of an iso-intensity shell was given by Augst *et al.* [29].

Analogue to the CMDs parallel to the z axis, the CMDs $D_{I_0}^{(\text{RDI})}(p_{1y}, p_{2y})$ can also be obtained by projecting the TDCS for laser-free electron impact ionization of the parent ion onto the minor polarization direction with the shift of drift momentum considered, i.e.,

$$p_{iy} = k_{iy} - A_y(t_r) \quad (i = 1, 2), \quad (20)$$

where $A_y(t_r)$ is the vector potential that corresponds to an electric field along the minor axis at the time t_r of recollision.

To gain insight into the asymmetry of the momentum distribution of ions observed in the experiments, we finally calculate the 2D momentum distribution $D_{I_0}^{(\text{ion})}(p_z, p_y)$ of ions for the RDI process, which is expressed by

$$D_{I_0}^{(\text{ion})}(p_y, p_z) = D_{I_0}^{(\text{ion})}(p_y) \times D_{I_0}^{(\text{ion})}(p_z), \quad (21)$$

where $D_{I_0}^{(\text{ion})}(p_z)$ and $D_{I_0}^{(\text{ion})}(p_y)$ are the one-dimensional (1D) momentum spectra for doubly charged ion Ne^{2+} along the major and minor axes obtained by projecting the CMDs $D_{I_0}^{(\text{RDI})}(p_{1z}, p_{2z})$ and $D_{I_0}^{(\text{RDI})}(p_{1y}, p_{2y})$ onto the main diagonals $p_{1z} = p_{2z}$ and $p_{1y} = p_{2y}$, respectively.

III. RESULTS AND DISCUSSION

Based on the above theory, we now turn to the simulation of CMDs and the momentum distributions of ions for NSDI of Ne with elliptically polarized laser pulses. In particular, we investigate the ellipticity-dependent asymmetry of the momentum distributions of Ne^{2+} ions for laser fields and parameters as applied in the measurements [10]. For these conditions, only the CMDs for laser-induced RDI are simulated.

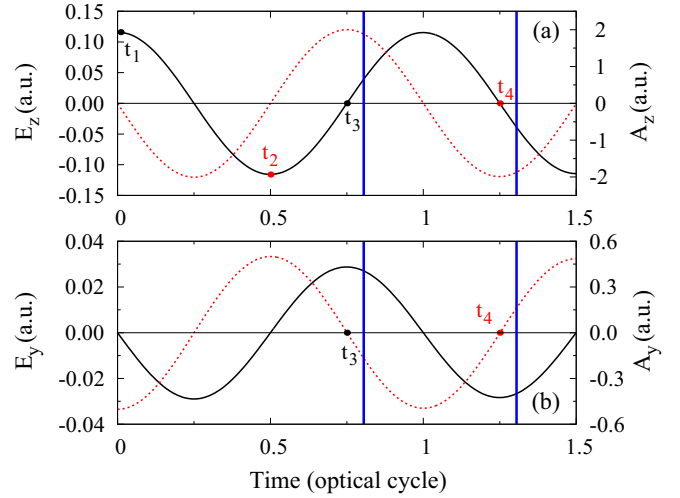


FIG. 1. Time information of the correlated electron emission in an elliptically polarized laser field at 788 nm with a peak intensity of $5.0 \times 10^{14} \text{ W/cm}^2$. The electric field (solid curve and left vertical axis) and vector potential (dotted curve and right vertical axis) along the major axis (the z axis) and the minor axis (the y axis) as a function of time are plotted in (a) and (b), respectively. The ellipticity is 0.25 here. The vertical lines show the recollision times after the E_z field zero crossing.

A. Time information of the correlated electron emission in elliptically polarized laser field

The observed ellipticity-dependent asymmetry of the momentum distributions of Ne^{2+} ions is owing to the strategy designed in the experiment for NSDI of Ne by using elliptically polarized electric fields [10]. As demonstrated in Fig. 1(a), according to the classical recattering model the first electron initially born near the peak of the laser field around t_1 (t_2) will return to the origin along $+\hat{z}$ ($-\hat{z}$) at a time around field crossing t_3 (t_4). Upon recollision of the returning (first) electron with the parent ion, the second electron may be ionized directly. Because the recollision time is around the E_z field zero crossing, the value of $A_z(t_r)$ at the recollision time is close to the peak vector potential, and the parallel momentum distributions along the major polarization are shifted to smaller (larger) momentum by $-A_z(t_r)$ when the first electron returns to the parent ion along $+\hat{z}$ ($-\hat{z}$) no matter whether recollisions occur before or after the field zero crossing. However, the situation becomes different for the momentum distributions along the minor polarization (y axis). Taking the case in which the first electron returns to the origin along $+\hat{z}$ at a time around field crossing t_3 as an example, both the y components of the final momenta of the two outgoing electrons will shift to negative or positive value if the recollision occurs before or after the E_z zero crossing, as one can see in Fig. 1(b). The great advantage of the experimental strategy is to measure the momentum distributions of Ne^{2+} ions in the y - z polarization plane of elliptically polarized laser pulses. It turns out that the recollisions are more likely to occur after the E_z zero crossing for higher ellipticities, leading to the asymmetric momentum distributions (see Fig. 2 in Ref. [10]).

In the improved QRS mode, an average return (recollision) time is used in the numerical calculations to take into account

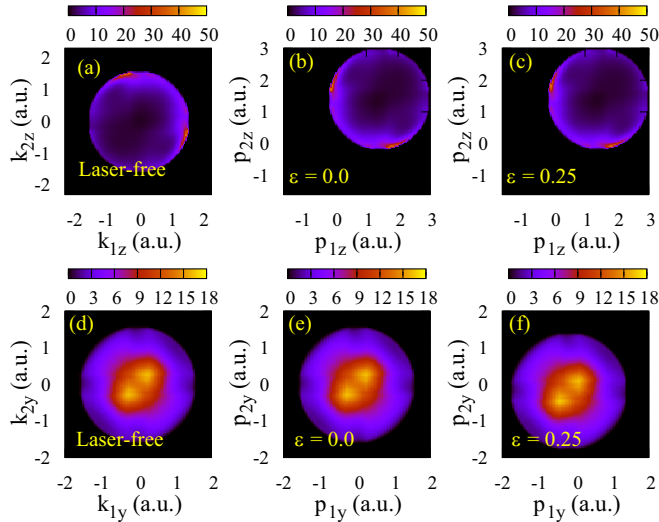


FIG. 2. Momentum distributions parallel to the z (top row) and y (bottom row) axes for two outgoing electrons in $(e, 2e)$ on Ne^+ at an incident energy of 75 eV for the laser-free process (left column) and the laser-induced RDI process of Ne in linearly polarized (middle column) and elliptically polarized (right column) laser pulses with a wavelength of 788 nm at a peak intensity of 5.0×10^{14} W/cm 2 for the situation where the recolliding electron returns to the origin along the $-\hat{z}$ direction.

the lowering of the threshold due to the presence of an electric field. As indicated by the vertical lines in Fig. 1, the average return time is chosen to be $\omega\Delta t_r = 20^\circ$ after the E_z field zero crossing since the probability for the first electron returns after the field zero crossing is much larger than that before the field zero crossing [30]. This is consistent with the experimental findings [10].

B. Parallel momentum distribution of electrons

Our ultimate goal is to simulate the momentum distributions of Ne^{2+} ions in the y - z polarization plane of elliptically polarized laser pulses. Following the numerical procedures presented in Sec. II(B), we first evaluate the CMDs along the major and minor polarizations, respectively. To this end, we need to prepare the TDCSs for laser-free $(e, 2e)$ process of Ne^+ which are calculated using the DWBA model, in which the incident direction is taken to be along the z axis. To account for the experimental measurements performed by Kang *et al.* [10], here, only the TDCSs for the two outgoing electrons in the y - z plane are evaluated. In Figs. 2(a) and 2(d) we show that the laser-free $(e, 2e)$ parallel momentum distributions along the z and y axes at an incident energy of 75 eV, respectively. In the parallel momentum distributions along the z axis, the electron pairs prefer to locate at the edge of the circle area with large momenta, while in the parallel momentum distributions along the y axis, the central part accommodates more electron pairs, indicating strong binary forward scattering in the $(e, 2e)$ process at the incident energy considered here. Figures 2(b) and 2(c) display the CMDs, obtained from the parallel momentum distributions shown in Fig. 2(a), for the laser-induced RDI process in NSDI of Ne in the laser fields with a wavelength of 788 nm at an intensity of

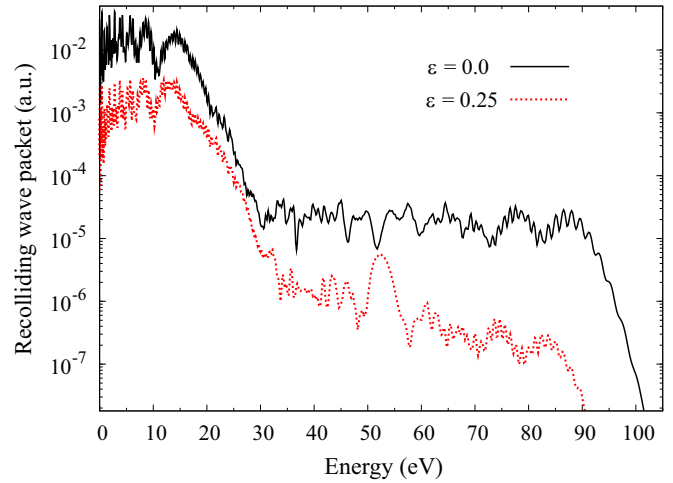


FIG. 3. Energy distribution of the recolliding wave packet $W_r(E_r)$ for the first returning electron computed from SFA2 for single ionization of Ne by 788 nm, 45 fs laser pulses at a peak intensity of 5.0×10^{14} W/cm 2 with ellipticities of 0.0 and 0.25, respectively.

5.0×10^{14} W/cm 2 with ellipticities of 0.0 and 0.25, respectively. For the situation where the recolliding electron returns to the origin along the $-\hat{z}$ direction, the CMDs in Figs. 2(b) and 2(c) are just a flip of the parallel momentum distribution for laser-free $(e, 2e)$ in Fig. 2(a), with the parallel momenta of the two electrons shifted by the drift momentum. According to Eq. (18), the parallel momentum shifts in Figs. 2(b) and 2(c) are 1.426 and 1.433, respectively. As a result, the CMD for RDI along the z axis in linearly polarized laser pulses is almost the same as that in elliptically polarized laser fields. Similarly, the CMDs along the y axis in Figs. 2(e) and 2(f) are obtained from that in Fig. 2(d). For linear polarization, $A_y \equiv 0$, the CMD for RDI in Fig. 2(e) is therefore exactly the same as the parallel momentum distribution for laser-free $(e, 2e)$ in Fig. 2(d). However, for elliptically polarized laser pulses, as demonstrated in Fig. 1, at the recollision time $A_y(t_r) = 0.171$ the CMD in Fig. 2(f) shifts to smaller momentum by $-A_y(t_r)$ with respect to that in Fig. 2(d). Therefore, the CMD along the minor polarization (y axis) unveils the details of the recollision more powerfully with elliptically polarized laser fields.

As will be explained below, the differences between the CMDs computed for zero and nonzero ellipticities clearly demonstrate that the drift momentum along the minor polarization axis plays a vital role in the formation of the asymmetric structural momentum distribution observed in the experiment.

For a given intensity, the RDI process could take place as long as the energy of the laser-induced electron exceeds the ionization potential. Therefore, integration of the CMDs over the incident energy has to be performed. For this purpose, one needs to evaluate the contribution weight for the recollision process at each incident energy. This weight is represented by the momentum (energy) distribution of RWP, which can be calculated using the SFA2 model [11] for HATI.

In Fig. 3 we present the RWPs as a function of the kinetic energy of the laser-induced returning electron with ellipticities of 0.0 and 0.25, respectively. Each wave packet starts with a fast drop at low energies before becoming roughly flat in

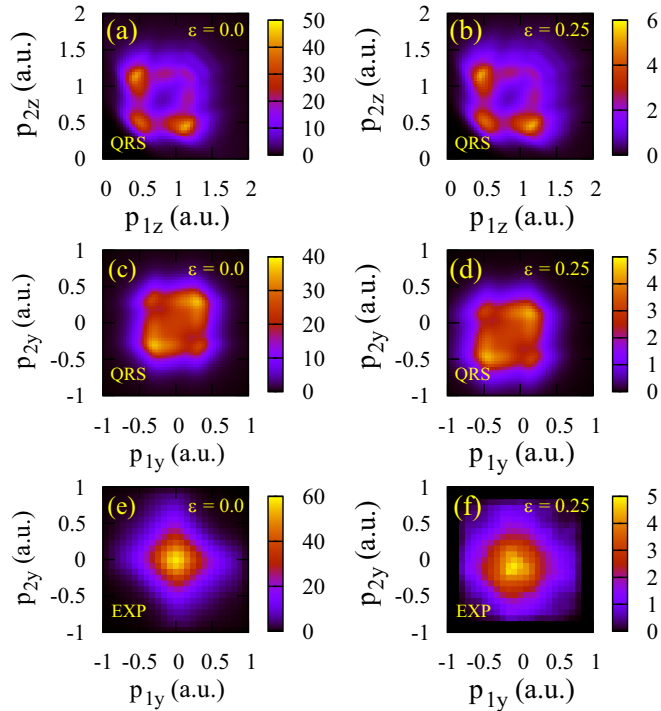


FIG. 4. Correlated two-electron parallel momentum distributions along the major (first row) and minor (second and third rows) polarization axes of the elliptically polarized light with ellipticities of 0.0 and 0.25, at a peak intensity of 5×10^{14} W/cm² and a wavelength of 788 nm for the situation where the recolliding electron returns to the origin along the $-\hat{z}$ direction. The focal volume averaging has been considered in the theoretical simulations using the QRS model displayed in the first and second rows. The experimental measurements displayed in the third row are taken from Ref. [10].

the plateau region with a cutoff at $3.17U_p$, where U_p is the ponderomotive energy. One can see from Fig. 3 that the RWP for linear polarization is roughly 10 times larger than the one for laser ellipticity of 0.25, which clearly indicates that the recollision is strongly suppressed for elliptical polarization. In addition, since the E_z field for elliptical polarization is smaller than that for linear polarization, the cutoff of the RWP, which is around 85.0 eV for ellipticity of 0.25, extends to a higher energy of 92.0 eV for linear polarization.

With the CMDs for all incident energies carefully prepared, the calculation of CMDs for the RDI process of Ne at an intensity is straightforward by performing the integration over the recollision energy in Eq. (16), in which the contributions from recollisions at all incident energies are considered. Here, the change of the threshold energy due to the presence of the electric field at the instant of recollision is taken into account as well. One more step in the numerical simulations is to perform the integration over the focal volume in Eq. (19) to ensure that the numerical results can be compared with the experimental measurements. After focal averaging, the final CMDs are obtained for the RDI process in NSDI of Ne in 45 fs and 788 nm laser pulses at a peak intensity of 5.0×10^{14} W/cm² with ellipticities of 0.0 and 0.25, respectively, which are displayed in Figs. 4(a)–4(d). We can see that similar to the results presented in Figs. 2(b) and 2(c), the focal-volume-

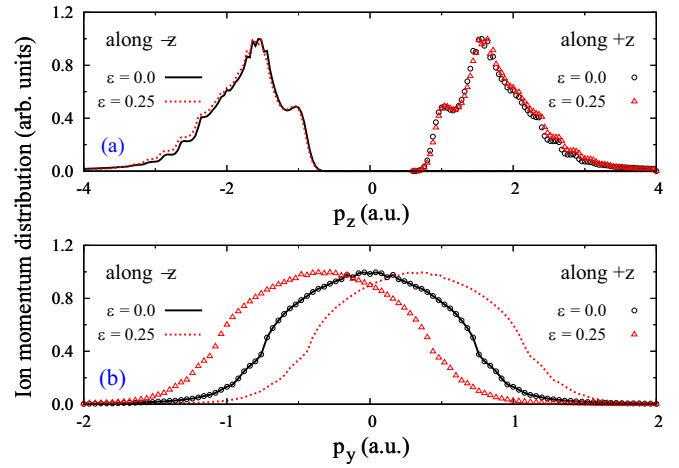


FIG. 5. Normalized ion momentum distributions along (a) the major and (b) the minor polarization axes of the elliptically polarized light with ellipticities of 0.0 and 0.25, at a peak intensity of 5×10^{14} W/cm² and a wavelength of 788 nm. The results for the situation where the recolliding electron returns to the origin along the $-\hat{z}$ direction are obtained by projecting the CMDs, displayed in Fig. 4, onto the main diagonals. See text for detail.

averaged CMDs along the major polarization axis in Figs. 4(a) and 4(b) are also located in the first quadrant for the situation where the recolliding electron returns to the origin along the $-\hat{z}$ direction. It is found that the maximum probabilities along the diagonal at $p_{1z} = p_{2z} \approx 0.5$ result from the contributions at energies below 60 eV, due to the fact that postcollision Coulomb interaction between the two outgoing electrons has not been taken into account in the present DWBA model. The postcollision interaction effect has already been proved important for ($e, 2e$) at low incident energies [31,32]. The simulated correlated two-electron parallel momentum distributions along the minor polarization in Figs. 4(c) and 4(d) are compared with the corresponding experimental measurements [10] in Figs. 4(e) and 4(f). The experimental measurements reveal that the probability of RDI drops dramatically and more electron pairs become located in the third quadrant of the CMD along the minor polarization axis as the ellipticity increases from 0 to 0.25. This trend is well reproduced by the present QRS model despite some discrepancies between theory and experiment.

C. Momentum distributions of Ne²⁺

The momentum distributions for the doubly charged ion Ne²⁺ along the major and the minor polarization axes of the elliptically polarized light for the situation where the recolliding electron returns to the origin along the $-\hat{z}$ direction can be obtained from the CMDs displayed in Fig. 4 by projecting the CMDs onto the main diagonals $p_{1z} = p_{2z}$ and $p_{1y} = p_{2y}$, respectively. The black solid and red dotted lines in Fig. 5 represent the obtained results for ellipticities $\varepsilon = 0.0$ and 0.25, respectively. As shown in Fig. 5, the ion momentum distributions for the situation where the recolliding electron returns to the origin along the $+\hat{z}$ direction (black circles and red triangles) mirror the distributions for the situation where the recolliding electron returns to the origin along the $-\hat{z}$

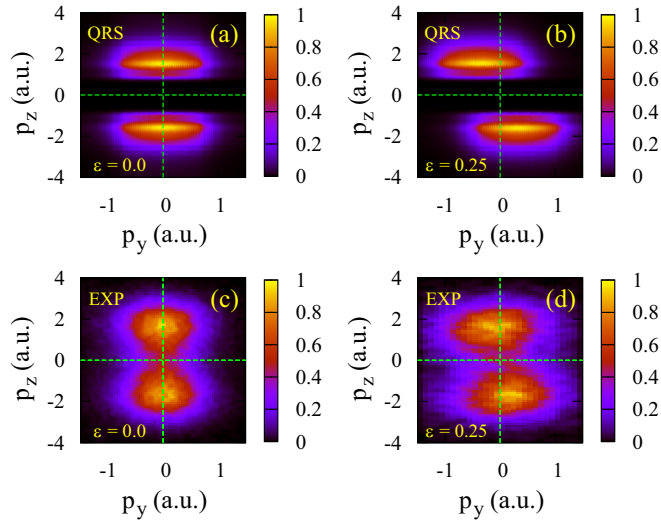


FIG. 6. Comparison of the momentum distributions of the theoretical simulations using the QRS model (top row) and the experimental measurements [10] (bottom row) for Ne^{2+} ions in the y - z polarization plane of elliptically polarized laser pulses at a peak intensity of 5.0×10^{14} W/cm² with a wavelength of 788 nm. The ellipticities are $\varepsilon = 0.0$ and 0.25 , respectively.

direction due to the fact that the two half cycles of the laser field yield opposite drift momenta.

One can see from Fig. 5(a) that the ion momentum distribution along the major polarization axis is independent of ellipticity since the normalized distributions for $\varepsilon = 0.0$ and 0.25 are almost identical. This is not surprising since the CMDs in Figs. 4(a) and 4(b) are almost the same except for the difference in magnitude. On the contrary, ellipticity plays an important role in the ion momentum distributions along the minor polarization axis. As demonstrated in Fig. 5(b), the ion momentum distribution shifts to larger momentum (absolute value) with increasing ellipticity. This is due to the fact that the larger the ellipticity, the larger drift momentum the two electrons gain along the minor polarization axis.

Finally, by multiplying the 1D ion momentum distributions along the major and minor polarization axes of the elliptically polarized light displayed in Figs. 5(a) and 5(b), respectively, we obtain the momentum distributions of Ne^{2+} ions in the y - z polarization plane which are displayed in Figs. 6(a) and 6(b). One can see from Fig. 5(a) that when the recolliding electron returns to the parent ion along the $-\hat{z}$ ($+\hat{z}$) direction, the Ne^{2+} ions locate in the lower (upper) half plane in the 2D momentum distributions in Figs. 6(a) and 6(b). Obviously, the probabilities of finding the Ne^{2+} ions in the lower half plane ($p_z < 0$) and the upper half plane ($p_z > 0$) are identical, whereas the second and fourth quadrants accommodate more Ne^{2+} ions with increasing ellipticity, which is in agreement with the experimental measurements [10] displayed in Figs. 6(c) and 6(d). The asymmetry between the first and second (or the third and fourth) quadrants is due to the hypothesis in the QRS model that the probability of the recollision occurring after the E_z field zero crossing is much larger than that before the E_z field zero crossing. While the validity of this hypothesis can hardly be tested with a linearly polarized laser

field, it is now unambiguously confirmed by the experiments with elliptically polarized lights [10].

IV. CONCLUSIONS AND OUTLOOK

Using the QRS model, we computed the CMDs of the two outgoing electrons and the momentum distributions of ions in NSDI of Ne by 788 nm laser pulses at a peak intensity of 5.0×10^{14} W/cm² with linearly and elliptically polarized laser fields, respectively. For the laser parameters considered here, we only took into account the RDI process of Ne^+ . The triple differential cross sections for laser-free electron impact ionization of Ne^+ were calculated with the DWBA model, and the momentum (energy) distributions for the returning electron wavepacket were evaluated within the strong field approximation.

In the present work, we have aimed to unveil the mechanisms for the symmetry in the momentum distribution of ions for linear polarization and the collapse of the symmetry in the momentum distribution of ions for elliptical polarization. Our study reveals that the drift velocity along the minor axis when the ellipticity is nonzero is responsible for asymmetric distribution for elliptical polarization. The overall good agreement between our model results and the experimental measurements confirms the basic assumptions of the QRS model, namely, that recollisions occur most probably after the E_z field zero crossing. This work provides guidelines for the study of NSDI with both linearly and elliptically polarized laser fields within the framework of the QRS model. Finally, it should be noted that without taking into account the RESI, the model fails to reproduce the ion momentum distributions in the range of $|p_z| < 0.7$. The agreement with the experiment could be improved if the contribution from RESI is considered.

Until the present, the QRS model has been used only for treating NSDI in linearly polarized laser fields. This work describes the first attempt to apply the QRS model to the study of NSDI in elliptically polarized laser fields. In recent years, many efforts have shifted to NSDI in elliptically polarized laser fields as well as counterrotating circularly polarized two-color fields [33–35], for which the semiclassical model has been widely employed. With the validity of the QRS model for dealing with NSDI in elliptically polarized laser fields established in this work, it is expected that the QRS model will become an efficient and effective tool to deal with NSDI in more complicated laser fields in the near future.

ACKNOWLEDGMENTS

This work was supported by the Deutsche Forschungsgemeinschaft (DFG, German Research Foundation) under Project No. 440556973. Z.C. acknowledges funding by the National Natural Science Foundation of China under Grant No. 11274219 and Guangdong Basic and Applied Basic Research Foundation, China, under Grant No. 2021A1515010047. F.L. wishes to thank Dr. Huipeng Kong for providing the experimental data plotted in Figs. 4 and 6 in digital form.

- [1] A. L'Huillier, L. A. Lompre, G. Mainfray, and C. Manus, *Phys. Rev. Lett.* **48**, 1814 (1982); *Phys. Rev. A* **27**, 2503 (1983).
- [2] D. N. Fittinghoff, P. R. Bolton, B. Chang, and K. C. Kulander, *Phys. Rev. Lett.* **69**, 2642 (1992).
- [3] B. Walker, E. Mevel, B. Yang, P. Breger, J. P. Chambaret, A. Antonetti, L. F. DiMauro, and P. Agostini, *Phys. Rev. A* **48**, R894 (1993).
- [4] B. Walker, B. Sheehy, L. F. DiMauro, P. Agostini, K. J. Schafer, and K. C. Kulander, *Phys. Rev. Lett.* **73**, 1227 (1994).
- [5] P. Dietrich, N. H. Burnett, M. Ivanov, and P. B. Corkum, *Phys. Rev. A* **50**, R3585 (1994).
- [6] F. Mauger, C. Chandre, and T. Uzer, *Phys. Rev. Lett.* **105**, 083002 (2010).
- [7] A. Kamor, F. Mauger, C. Chandre, and T. Uzer, *Phys. Rev. Lett.* **110**, 253002 (2013).
- [8] X. Wang and J. H. Eberly, *New J. Phys.* **12**, 093047 (2010).
- [9] X. Wang and J. H. Eberly, *Phys. Rev. Lett.* **105**, 083001 (2010).
- [10] H. Kang, K. Henrichs, M. Kunitski, Y. Wang, X. Hao, K. Fehre, A. Czasch, S. Eckart, L. Ph. H. Schmidt, M. Schöffler, T. Jahnke, X. Liu, and R. Dörner, *Phys. Rev. Lett.* **120**, 223204 (2018).
- [11] Z. Chen, A.-T. Le, T. Morishita, and C. D. Lin, *Phys. Rev. A* **79**, 033409 (2009).
- [12] Z. Chen, A.-T. Le, T. Morishita, and C. D. Lin, *J. Phys. B: At. Mol. Opt. Phys.* **42**, 061001 (2009).
- [13] Z. Chen, Y. Liang, and C. D. Lin, *Phys. Rev. Lett.* **104**, 253201 (2010).
- [14] Z. Chen, Y. Liang, and C. D. Lin, *Phys. Rev. A* **82**, 063417 (2010).
- [15] Z. Chen, F. Liu, H. Wen, T. Morishita, O. Zatsarinny, and K. Bartschat, *Opt. Express* **28**, 22231 (2020).
- [16] F. Liu, Z. Chen, T. Morishita, K. Bartschat, B. Böning, and S. Fritzsche, *Phys. Rev. A* **104**, 013105 (2021).
- [17] P. B. Corkum, *Phys. Rev. Lett.* **71**, 1994 (1993).
- [18] B. Feuerstein, R. Moshhammer, D. Fischer, A. Dorn, C. D. Schröter, J. Deipenwisch, J. R. Crespo Lopez-Urrutia, C. Höhr, P. Neumayer, J. Ullrich, H. Rottke, C. Trump, M. Wittmann, G. Korn, and W. Sandner, *Phys. Rev. Lett.* **87**, 043003 (2001).
- [19] Z. Chen, Y. Liang, D. H. Madison, and C. D. Lin, *Phys. Rev. A* **84**, 023414 (2011).
- [20] Z. Chen, F. Liu, and H. Wen, *Chin. Phys. B* **28**, 123401 (2019).
- [21] Z. Chen, T. Morishita, A.-T. Le, and C. D. Lin, *Phys. Rev. A* **76**, 043402 (2007).
- [22] B. Böning, W. Paufler, and S. Fritzsche, *Phys. Rev. A* **99**, 053404 (2019).
- [23] X. M. Tong and C. D. Lin, *J. Phys. B: At. Mol. Opt. Phys.* **38**, 2593 (2005).
- [24] Z.-J. Lai, D.-F. Chen, L.-Q. Pan, X.-H. Jiang, Y.-L. Xu, and Z.-J. Chen, *J. At. Mol. Sci.* **5**, 311 (2014).
- [25] O. Zatsarinny, H. Parker, and K. Bartschat, *Phys. Rev. A* **99**, 012706 (2019).
- [26] X. Ren, I. Bray, D. V. Fursa, J. Colgan, M. S. Pindzola, T. Pflüger, A. Senftleben, S. Xu, A. Dorn, and J. Ullrich, *Phys. Rev. A* **83**, 052711 (2011).
- [27] Y. Liang, Z. Chen, D. H. Madison, and C. D. Lin, *J. Phys. B: At. Mol. Opt. Phys.* **44**, 085201 (2011).
- [28] H. W. van der Hart and K. Burnett, *Phys. Rev. A* **62**, 013407 (2000).
- [29] S. Augst, D. D. Meyerhofer, D. Strickland, and S. L. Chin, *J. Opt. Soc. Am. B* **8**, 858 (1991).
- [30] Z. Chen, Y. Wang, L. Zhang, and X. Jia, *Phys. Rev. A* **99**, 033401 (2019).
- [31] A. Prideaux, D. H. Madison, and K. Bartschat, *Phys. Rev. A* **72**, 032702 (2005).
- [32] X. Ren, T. Pflüger, J. Ullrich, O. Zatsarinny, K. Bartschat, D. H. Madison, and A. Dorn, *Phys. Rev. A* **85**, 032702 (2012).
- [33] J. L. Chaloupka and D. D. Hickstein, *Phys. Rev. Lett.* **116**, 143005 (2016).
- [34] C. A. Mancuso, K. M. Dorney, D. D. Hickstein, J. L. Chaloupka, J. L. Ellis, F. J. Dollar, R. Knut, P. Grychtol, D. Zusin, C. Gentry, M. Gopalakrishnan, H. C. Kapteyn, and M. M. Murnane, *Phys. Rev. Lett.* **117**, 133201 (2016).
- [35] S. Eckart, M. Richter, M. Kunitski, A. Hartung, J. Rist, K. Henrichs, N. Schlott, H. Kang, T. Bauer, H. Sann, L. Ph. H. Schmidt, M. Schöffler, T. Jahnke, and R. Dörner, *Phys. Rev. Lett.* **117**, 133202 (2016).